Thin Solid Films 612 (2016) 437–444

Contents lists available at ScienceDirect

Thin Solid Films

journal homepage: www.elsevier.com/locate/tsf

Simulation of phase transformation kinetics in thin films under a constant nucleation rate

M.M. Moghadam [a,*], E.L. Pang [a], T. Philippe [b], P.W. Voorhees [a]

[a] Department of Materials Science and Engineering, Northwestern University, Evanston, IL 60208, USA
[b] Condensed Matter Physics, Ecole Polytechnique, CNRS, 91128 Palaiseau, France

ARTICLE INFO

Article history:
Received 26 January 2016
Received in revised form 30 May 2016
Accepted 16 June 2016
Available online 17 June 2016

Keywords:
Thin film
Kinetics
Phase transformation
Crystallization
Constant nucleation rate
JMAK theory
Level-set method

ABSTRACT

The classic framework of Johnson-Mehl-Avrami-Kolmogorov (JMAK) has been commonly used in studies of thin film phase transformation kinetics despite its inherent limitation to transformations that occur in finite size domains or via heterogeneous nucleation on surfaces. To address the effects of finite size and heterogeneous nucleation on a JMAK analysis, we employ the level-set method to simulate phase evolution in thin film systems. Isothermal transformations under a constant nucleation rate and isotropic interface growth, with both bulk and surface nucleation cases are considered for broad range of film thicknesses. In agreement with past work, we find that when the thickness of the film is sufficiently small or heterogeneous nucleation on surface is present, it is possible to have a non-constant Avrami exponent over the course of phase transformation. Our results also show that the rate constant varies with the film thickness in contrast to bulk phase transformations. Furthermore, we obtain the grain size distributions at the end of the transformation for various film thicknesses that vary strongly in shape for small changes in film thickness when the film thickness is on the order of the characteristic length. By analyzing this information and determining the change of the average grain size with film thickness, we find that, the film thickness relative to the characteristic length is a reliable indicator of the dominant growth dimensionality in thin film phase transformations.

1. Introduction

A phase transformation theory proposed by Johnson, Mehl, Avrami and Kolmogorov (JMAK) in late 30s has been used extensively as a classic framework for describing nucleation and growth kinetics in different materials systems. However, any constraint on system size or homogeneity of nucleation may violate the governing assumptions used in deriving the JMAK equation and thus lead to a departure from expected behavior [1–5].

The core idea of JMAK theory is articulated as an exponential dependence of the transformed volume fraction (f_V) on time (t) with two coefficients [6–10],

$$f_V = 1 - \exp(-kt^n) \tag{1}$$

where k is a temperature-dependent rate constant and n is the Avrami exponent. To extract the Avrami exponent and rate constant from experimental data, Eq. (1) can be rewritten as

$$\ln[-\ln[1-f_V]] = \ln[k] + n\ln[t] \tag{2}$$

Using this relation one can plot $\ln[-\ln[1-f_V]]$ versus $\ln[t]$, which is known as Avrami plot. When the assumptions of the JMAK equation are all met, this plot is linear with a slope equal to the Avrami exponent (n) and a y-intercept (at $\ln[t]=0$) equal to $\ln[k]$. The avrami exponent is traditionally used to determine the dimensionality (D) of the growth. For phenomena with constant nucleation rate kinetics, the Avrami exponent is expected as $n = D + 1$, while for site saturated nucleation it equals D [11].

Despite its simplicity, JMAK equation captures the kinetics of nucleation and growth phase transformation in many bulk materials where the transformation occurs with a constant crystallographically isotropic interfacial velocity. However, several experimental results have shown serious deviations from Eq. (2), particularly for systems with a finite size. Thus, for most phase transformations occurring in thin films, it is very difficult to satisfy the assumptions of the JMAK theory [1,5,12–15]. The mixed dimensionality of thin film growth causes growing particles to soon impinge upon the free surface and violate infinite size assumption. Surface nucleation, which is often energetically favorable, also complicates the analysis of phase transformation kinetics using the classical JMAK approach.

These limitations of JMAK equation have been frequently addressed in literature [12–24]. In general there is a consensus that there should be a lower Avrami exponent in systems with finite size. It has been also

* Corresponding author.

http://dx.doi.org/10.1016/j.tsf.2016.06.035
0040-6090/

observed that the Avrami exponent is not constant over the course of transformation. Furthermore, the results of models of phase transformations that occur via heterogeneous nucleation suggest reduced Avrami exponents, as well [12,15,16,21,25–27]. Beside the aforementioned studies, different attempts have also been made to extend JMAK equation to account for these effects [21,23]. Despite these efforts, the lack of a simple and comprehensive replacement for the JMAK analysis keeps this field as an active area of research.

We develop a computational approach employing the level-set method to explore phase transformation kinetics within thin films, under a constant nucleation rate. The level-set method brings a unique capability to conduct a systematic study of thin film phase transformations for broad range of film thicknesses and nucleation origins. Simulation results provide new insights on different aspects of thin-film phase transformation kinetics, including the evolution of the Avrami exponent over time, the dependence of the rate constant on the film thickness and the growth dimensionality.

This paper is organized as follows. In Section 2, we discuss constant nucleation rate and define characteristic length and time for this mechanism. In Section 3, we outline our simulation methodology based on level-set method. In Section 4, we highlight our results for bulk and surface nucleation cases. In Section 5, we discuss the results in further details. Section 6 contains a brief summary of main findings.

2. Constant nucleation rate

We assume a constant nucleation rate ($\dot{N}_V$) where $\dot{N}_V$ is the number of nuclei per untransformed volume per time. To make a meaningful comparison between different systems, the kinetics of a given system is described using characteristic length and time scales [15,16]. The characteristic length (λ) is:

$$\lambda = \left(\frac{\dot{N}_V}{v}\right)^{-1/4} \tag{3}$$

where v is the constant interface growth velocity in normal direction. The characteristic length encompasses a competition between nucleation and growth, which can reveal basic information regarding final average grain size [28]. The characteristic time scale (τ) is defined as:

$$\tau = \frac{\lambda}{v} \tag{4}$$

These characteristic length and time scales are then used to scale all the dimensional quantities of the system. In this manuscript, * is used to denote all non-dimensional quantities, e.g. the relative film thickness $h^* = h/\lambda$. In these dimensionless variables, $\dot{N}_V{}^* = 1$, $\dot{N}_V{}^* = 1$ and $v^* = 1$.

3. Simulation methodology

The level-set method [29,30] is a geometrical scheme to predict complicated evolution of fronts and interfaces over the time and is an ideal approach to simulate interface-controlled phenomena such as crystallization, chemical and ion dissolution, eutectic growth, cellular precipitation and discontinuous coarsening [31]. It is, in particular, suitable to follow particle coalescence as well as contact with the external domain [32–34]. Interfacial evolution on experimental length and time scales is another advantage of using level-set method, which makes its results directly comparable with phase transformation experiments [29,30].

In the current paper, we use a level-set method to simulate a phase transformation with isotropic interfacial velocity in a thin film. A level-set function (ϕ) is defined such that $|\nabla\phi| = 1$. Here, ϕ is a signed distance function wherein it is negative inside a particle (transformed region), and positive outside the particle (untransformed region). The interface between the transformed and untransformed region is thus $\phi = 0$. Isotropic growth is achieved by defining a velocity field as a constant motion in the direction normal to the interface $\vec{V} = v\vec{N}$, where v is constant interface velocity and $\vec{N}$ is a normal vector to the interface. The equation of motion of the level-set function for the assumed velocity field is

$$\frac{\partial\phi}{\partial t} + v|\nabla\phi| = 0. \tag{5}$$

Forward Euler time discretization is then employed to track the evolution of ϕ over time explicitly in 3D Cartesian meshed domain as follow:

$$\phi^{t+1} = \phi^t - v\Delta t \tag{6}$$

For all examined cases, a uniform mesh space and time step are used: $\Delta x^* = \Delta y^* = \Delta z^* = 10^{-2}$ and $\Delta t^* = 10^{-2}$ respectively. In each time step, the volume with negative ϕ value is determined in order to track the transformed volume. The local Avrami exponent n, is then numerically extracted from Eq. (2) by applying a five-point stencil derivative using following equation [35]:

$$n = \frac{d\ln[-\ln[1-f_v]]}{d\ln[t]} \tag{7}$$

To verify this approach, a 3D simulation of a phase transformation was used with a constant nucleation rate and compared with the JMAK predictions. Periodic boundary conditions were imposed in all directions and nuclei were adding to the system homogenously to satisfy all assumptions of JMAK theory. For all data presented in the verification section, which is taken as a function of volume fraction evolution, the average standard deviation is 10^{-2} to 4.1×10^{-3} for system volumes ranging from 100 to 400. These values provide a measure of the spread of the simulation results around an average value. For each data point, 40 independent runs were averaged.

Fig. 1(a) plots the Avrami exponent versus volume fraction transformed for the 3D phase transformation process [35], for different system volumes. The Avrami exponents from the simulation are relatively constant and equal to four as expected from JMAK theory. The slight discrepancy in n at the end of the transformation is a result of the final stages of the phase transformation in a finite system, since the final stages of the transformation do not follow the random impingement assumed in the classical JAMK theory [13,14]. We will address this phenomenon in detail at discussion section. Avrami plots of the simulation results shown in Fig. 1(b) display a linear regime with a slope of four, corresponding to the Avrami exponent, in agreement with JMAK theory. As it is shown in Eq. (2), the y-intercept in Avrami plot is equal to $\ln[k]$. From the simulation results we find $k^* = 1.04\mp0.03$. In three dimensions with constant nucleation rate, the rate constant is $k = \frac{\pi}{3}v^3\dot{N}_V$, which yields the JMAK equation in dimensionless form as [14,17]:

$$f_V = 1 - \exp\left[-\frac{\pi}{3}t^{*4}\right] \tag{8}$$

Therefore, in theory, k^* is expected to be $\pi/3$ ($=1.047$). This is again in reasonable agreement with JMAK theory, thus verifying our computational approach.

A broad range of film thicknesses (0.2–10) is examined to investigate effects of film thickness on the phase transformation kinetics. For $h^* \geq 1$, the size of x-y plane is fixed as 10×10, while for $h^* < 1$, the size of x-y plane is adjusted to set the total volume as 100. The number of required nuclei is added to the untransformed phase is based on the available untransformed volume in every characteristic time. Periodic

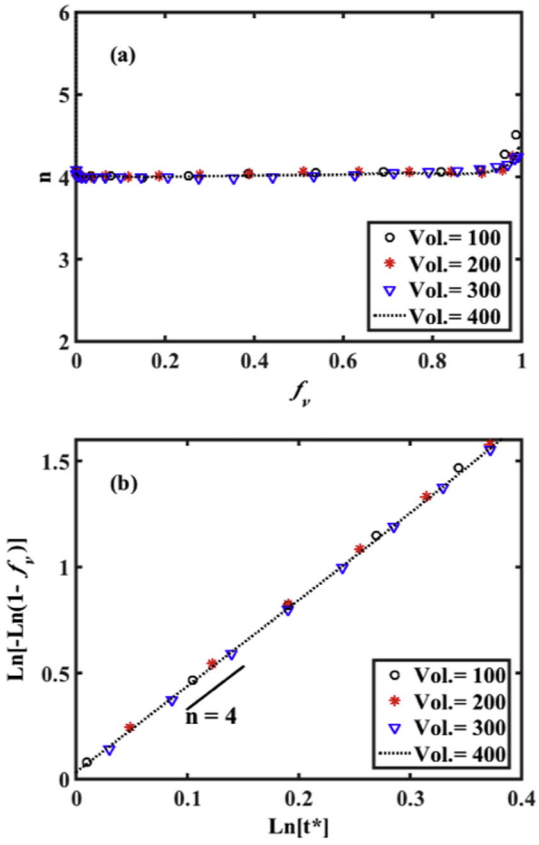

Fig. 1. Evolution of Avrami exponent in different system size. (a) Avrami exponent vs. volume fraction transformed. (b) Avrami plot. Results are in reasonable agreement with the predictions of JMAK theory. Solid line demonstrates the slope associated with $n=4$. Average values over 40 runs with different random initial configurations are displayed.

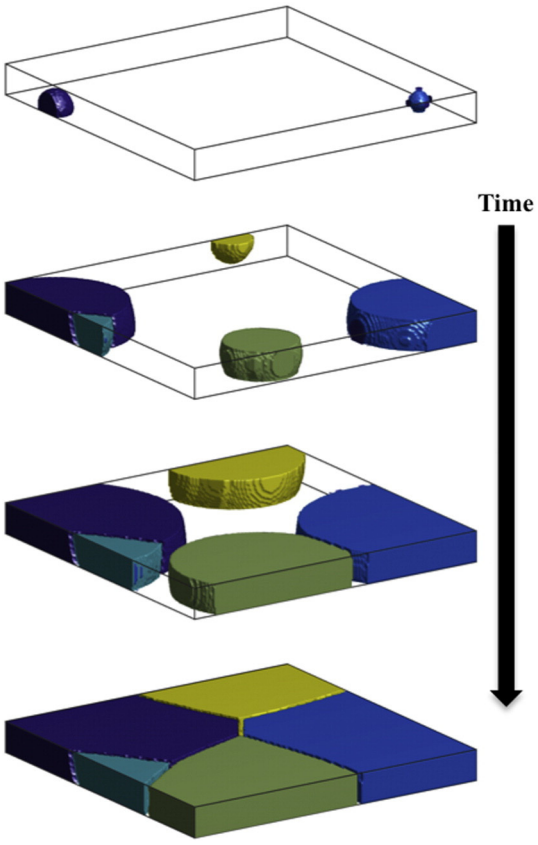

Fig. 2. Visualization of a phase transformation process modeled by the level-set method for bulk nucleation case with $h^*=0.2$, shown is a small section of $(2\times2\times0.2)$ of a larger system. The transformed volume has been shown.

boundary conditions are also imposed in lateral sides (x, y directions) but not in z direction, since the film thickness is the z-direction.

4. Results

A phase transformation in a thin film can initiate either from the surface or inside the film. We thus, present the results for bulk and surface nucleation separately.

4.1. Thin film bulk nucleation

In thin film bulk nucleation case, nuclei can appear everywhere inside the thin film over the course of simulation. Calculation of the Avrami exponent shows that for all h^*, the initial value begins at four which is consistent with the value obtained for a constant nucleation rate in 3D unbounded bulk. As the new phase hits the surfaces of the thin film (see Fig. 2), the Avrami exponent starts to decrease toward three due to a change in growth dimensionality from 3D to 2D. Although this behavior is more or less observed in all cases, two distinct regimes can be identified as h^* gradually increases. For smaller h^*'s in Fig. 3(a), there is a region after the initial growth where the growth is roughly 2D with Avrami exponents close to 3. However for larger film thicknesses, 3D growth is dominant with an Avrami exponent around 4. This is qualitatively in agreement with Očenášek et al.'s [17] analytical model that suggests 2D kinetics will be present for $h^*<0.3$ and 3D kinetics will be operative for $h^*>10$. The Avrami plot in Fig. 3(b) highlights these two regimes as well. The lines for higher thickness ($h^*\geq5$) almost coincide, with the slope relatively close to $n\approx4$, a characteristic of 3D growth. For smaller h^* values, the Avrami exponent is decreasing gradually until reaching the value consistent with the characteristic of 2D growth ($n=3$) at $h^*=0.2$.

The high values of the local Avrami exponent, observed in the first few time steps in the local Avrami exponent plots are caused by the relatively large changes in volume fraction evolution over the time. This issue can be remedied by using a smaller time step and consequently finer mesh, but this significantly increases computation time. For all data presented in this section, which is taken as a function of volume fraction evolution, the average standard deviation is 1.3×10^{-2} to 4.3×10^{-3} for film thicknesses ranging from 0.2 to 10. These values provide a measure of the spread of the simulation results around an average value. For each data point, 40 independent runs were averaged.

The Avrami plot also shows the obvious variation of the rate constant (y-intercept at $\ln[t^*]=0$) with respect to the film thickness. For larger h^* values, the rate constant is $k\approx\pi/3$ as predicted by Eq. (8) for 3D growth in bulk. However in thinner films, rate constant decreases by film thickness [17] to $k=\pi h^*/3$. This is consistent with the predominant 2D growth of the transformed phase, after early impingement at the surface that prevents 3D growth. This trend is better highlighted in Fig. 4, which demonstrates how the rate constant evolves as the film thickness increases. The two distinguishing behaviors, which are highlighted earlier, are more evident here. The rate constant for $h^*\gg1$ asymptotes to $\pi/3$, which means that as the film gets thicker, 3D growth plays more dominant rule in transformation. On the other side, for $h^*<1$, the rate constant follows approaches $k=\pi h^*/3$, which indicates more 2D growth as film gets thinner. Transition between these two regimes occurs smoothly around $h^*=1$. Considering the fact that the rate constant in JMAK theory counts for extended volume (ignoring the impingement) over the course of the transformation, this change in rate constant can lead to the new insight regarding the growth dimensionality.

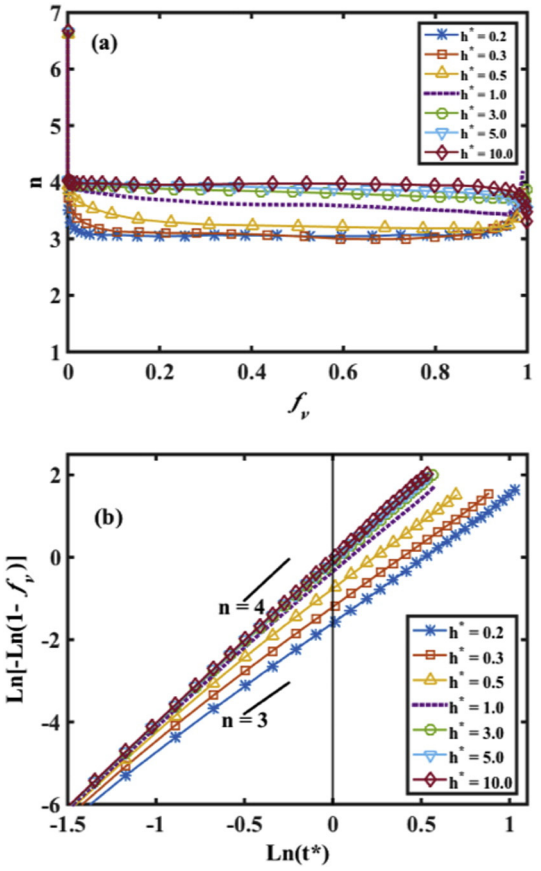

Fig. 3. Evolution of Avrami exponent as a function of h^* for bulk nucleation case. Average values over 40 runs with different random initial configurations are displayed. (a) Avrami exponent vs. volume fraction transformed. (b) Avrami plot. Fine solid line at $\ln[t^*]=0$, highlights different y-intercept as an indication of different rate constant. Solid lines demonstrate the slope associated with given n.

As discussed above, inferring the growth dimensionality from the Avrami exponent results in the condition that indicates the 2D growth for $h^* \le 0.3$ and 3D growth for $h^* \ge 10$. However investigating the rate constant evolution indicates that the growth dimensionality in thin film never reflects an absolute 2D or 3D kinetics over a wide range of the film thicknesses. Though it is possible to define a dominant growth mechanism as a function of the relative film thickness. To analyze the growth dimensionality further, we take advantage of the level-set simulation to determine the grain size distribution at the end of the transformation. We find that the thickness of the film has a major influence on grain size distribution. Fig. 5(a) shows the probability density of finding a grain of a given size for different h^*. Two distinguished regimes are evident. For $h^*<1$, a relatively sharp peak with high probability in the limited range of $1 \le d^* \le 1.5$ is observed, while for $h^* \ge 1$, humped shape, with a broader peak and approximately similar probability for $0.5 \le d^* \le 2$ is seen. Interestingly, there is a significant, but smooth, change in the grain size distribution on crossing $h^*=1$. These distributions are very different from those observed during classical grain growth in bulk system [36]. Total number of grains (N_{grn}) used to generate grain size distribution ranges from 6097 to 25,342 for $h^*=0.2$ and $h^*=10$ respectively. Bin size is scaled as $N_{grn}^{-1/3}$, which has been proven as an optimal bin size for representing the large number of data with a compact distribution [37,38]. The non-zero probability of grain size less than zero in Fig. 5(a) is generated by a kernel-smooth density estimate and is not present in the actual simulation results.

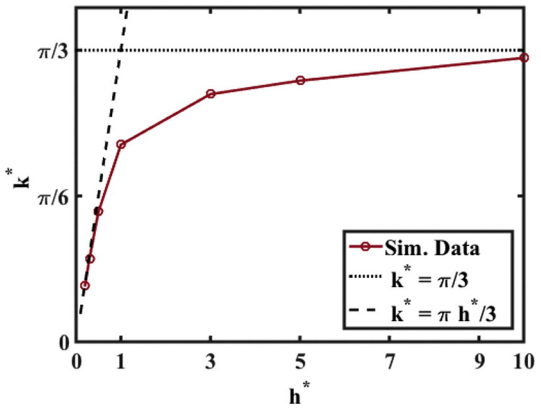

Fig. 4. Variation of rate constant (k^*) with film thickness (h^*). Average values over 40 runs with different random initial configurations are displayed.

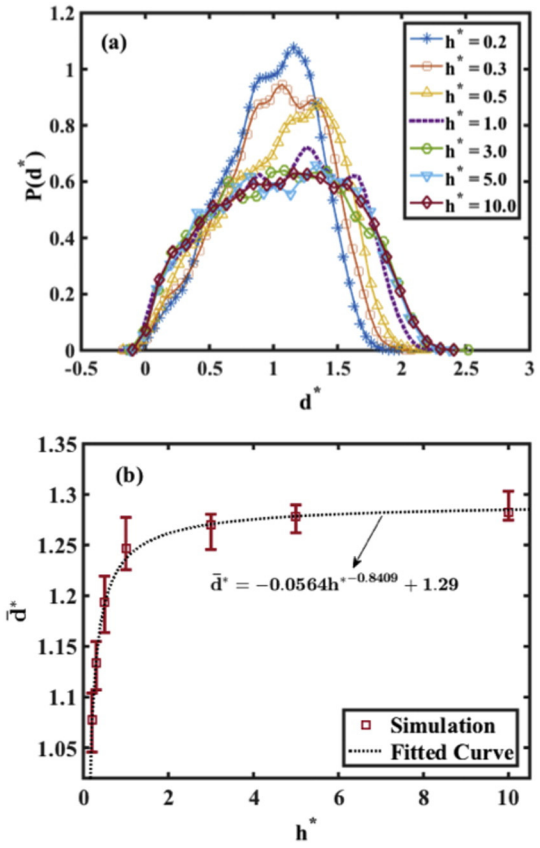

Fig. 5. (a) Probability density of grain size distribution for different film thicknesses. (b) Average grain size ($\bar{d}^*$) as a function of film thickness.

In Fig. 5(b), we show the change of the average grain size ($\bar{d}^*$) with h^*. The average grain size was determined using a spherically equivalent volume ($\bar{d}^* = 2\sqrt[3]{3\bar{V}^*/4\pi}$) where $\bar{V}^*$ is the average grain volume. Eq. (9) represents a reasonable fit to the data shown in Fig. 5(b).

$$\bar{d}^* = -0.0564\, h^{*-0.8409} + 1.29 \tag{9}$$

Interestingly this plot shows the same trend as seen for rate constant (Fig. 4). For $h^*>1$, the average grain size asymptotes to 1.29, which is the value for an infinite system as given by JMAK theory [9] and in agreement with Očenášek et al.'s [17] estimate for the average grain size for 3D growth of $\bar{d}^* = 1.28$. At lower thicknesses ($h^*<1$), the average grain size shows a strong dependence on film thickness. In this range, our average grain size values are lower than Očenášek et al.'s [17] prediction for 2D growth. For instance at $h^*=0.3$, our result shows $\bar{d}^* = 1.13$ while their prediction is 1.76. This discrepancy caused by their

assumption of absolute 2D growth, leads them to use the average surface area instead of the average volume in grain size calculation. However, one can convert their 2D result to 3D by assuming a cylindrical shape for each grain and incorporating the film thickness in volume estimation. For example for $h^*=0.3$ we find using the 3D definition of grain size that Očenášek's result [17] yields $\bar{d}^* = 1.11$, which is consistent with our finding. However the large difference in the initial grain size calculation (>50%) shows that the assumption of absolute 2D growth in this range can lead to an inaccurate result, even in films with small h^* values. This also emphasizes how care must be exercised in interpretation of grain size data, especially when they are extracted from the experiment.

The present connection between final average grain size and film thickness enables us to determine the characteristic length of an experiment by substituting measured $\bar{d}$ and h in Eq. (9) and solving for λ numerically. Taken together, all of the aforementioned results indicate a significant distinction between growth dimensionality of thin film phase transformations when the thickness is above or below the characteristic length. This new criterion defines predominant growth mechanism as two-dimensions for $h^*<1$ and three-dimensions for $h^*\geq 1$. This is in qualitative agreement with Teran et al.'s [39] analytical model that predicts that when the film thickness is smaller than the average grain size, the kinetics of the transformation is best described as 2D, while as film thickness increases beyond the final average grain size, 3D growth offers a better description.

4.2. Thin film surface nucleation

Occasionally phase transformations begin from either the surface of a thin film or the interface with the substrate. It is also possible that nucleation takes place at both surfaces simultaneously. Thus, we consider both scenarios of one or two surface nucleation to investigate effect of h^*on the kinetics of the phase transformation in thin films.

Fig. 6 shows time evolution of phase transformation process for the one and two-surface nucleation cases. The Avrami exponents for these two scenarios are presented in Figs. 6 and 7. Interestingly, both scenarios show similar behavior with only slight differences in time and growth dimensionality. For all simulations, the Avrami exponent starts from four, due to the relatively unconstrained growth of particles in 3D. As transformation evolves in time, three different regions can be seen. For $h^*\leq 0.5$, the Avrami exponent decreases toward three, which is an indicator for 2D kinetics. For $h^*\geq 3$, there is a decrease in the Avrami exponent toward two and even lower values, which indicates transition

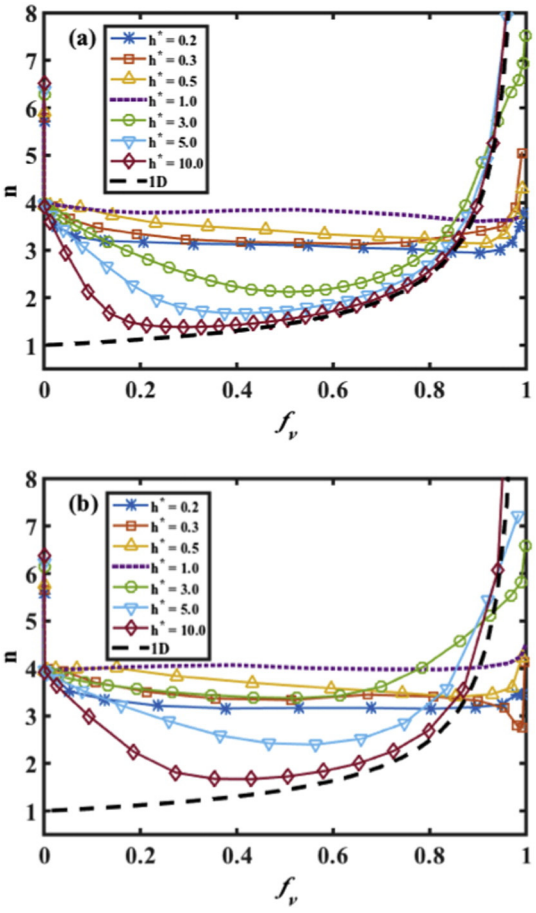

Fig. 7. Evolution of the Avrami exponent as a function of h^* for the surface nucleation case. Average values over 40 runs with different random initial configurations are displayed. (a) Avrami exponent vs. volume fraction transformed (1-surface case). (b) Avrami exponent vs. volume fraction transformed (2-surface case). Dashed line represents solution for a 1D planar front.

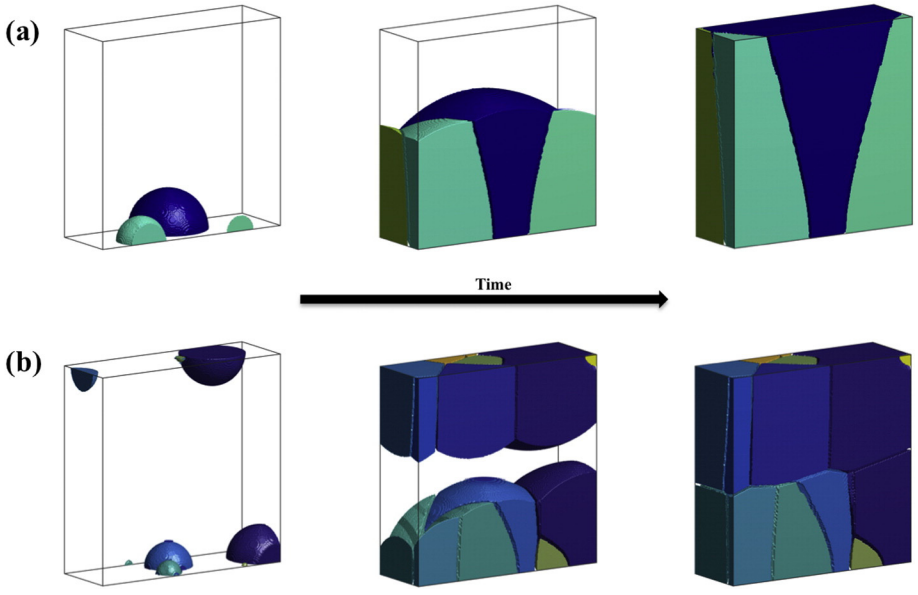

Fig. 6. Visualization of phase transformation evolution in time for surface nucleation, $h^*=3.0$, section view (3×1×3) (a) 1-surface case and (b) 2-surface case (transformed volume fraction has been shown).

from 3D to 1D growth. To highlight this transition, an analytical solution for 1D growth is also plotted in Fig. 7(a) and (b) [24,25]. Clearly, at sufficiently long time all film thicknesses follow 1D growth and this behavior becomes more pronounced when h^* is larger. Among all these simulations, $h^*=1$ shows a unique trend with no major deviation from initial value. This behavior is also evident in Fig. 8(a) and (b) as this case yields the only straight line (with a slope near four) in Avrami plot, which is consistent with the constant Avrami exponent in n vs. f_v plot. Changes in the slope for samples with $h^*\geq 3$ is obviously more pronounced than for thinner films ($h^*\leq 0.5$) as mentioned before. A set of parallel lines shown in Fig. 8(a) and (b) at early time represents a short period of time at the beginning of all simulations that yield the same Avrami exponent.

A better understanding of the aforementioned phenomena can be achieved by monitoring Avrami exponent over time, as shown in Fig. 8(c) and (d). For relatively small h^* simulations ($h^*\leq 0.5$), the departure from 3D kinetics starts when the first grain touches the surface. After contacting the surface the growth becomes 2D for a given grain, which leads to a decrease in the Avrami exponent of the overall transformation, see Fig. 8(c) and (d). As the number of impingements between grains contacting the surface increases, the Avrami exponent decreases. However, since free growth from the untransformed surface continues as a consequence of constant nucleation rate, the overall Avrami exponent for relatively small h^* never reaches three.

For simulations with $h^*\geq 3$, the higher film thickness implies a longer time for the 3D growth before reaching other side and starting the 2D growth. However, at the same time nucleation and growth continues on the surface until the transformed phase covers the entire surface(s). At this point, nucleation on the surface(s) is stopped and all grains form a relatively flat front that then grows in one direction toward opposite surface (Fig. 6, intermediate stage). This causes a rapid decrease in the Avrami exponent from four to that of 1D kinetics (two and lower). These observations are in agreement with Sun et al.'s [27] analytical prediction that the surface nucleation leads to a decrease in n during a transformation process. For special case of $h^*=1$, system characteristic length (λ) is comparable to the film thickness, which implies unconstrained growth in three dimensions that transforms most of the system before grains start to impinge the surface(s). Therefore, 2D and 1D kinetics would not be able to contribute in this process significantly. As a result, the phase transformation advances with 3D kinetics almost entire run. For all data presented in this section, which is taken as a function of volume fraction evolution, the average standard deviation is 1.4×10^{-2} to 8.6×10^{-4} for film thicknesses ranging from 0.2 to 10. These values provide a measure of the spread of the simulation results around an average value. For each data point, 40 independent runs were averaged.

As mentioned earlier, the general behavior of the phase transformation in both cases including one and two-surface nucleation are similar, however some differences are still observable. Obviously, the total time for a complete transformation is smaller in the two-surface nucleation case because transformation initiates from both surfaces simultaneously. It is also evident that the two-surface simulations show less 1D character at a given f_v, since they have less space available to form relatively flat advancing fronts. In two-surface samples, the average grain size is smaller and the grains show a more uniform morphology than in one-surface samples (Fig. 5, final stage).

5. Discussion

Simulation results clearly show that the finite size of the system can lead to a non-linear regime in the Avrami plot. In a case of homogeneous nucleation (Section 4.1), the non-linear behavior is mostly seen at the end of transformation in film thickness less than characteristic length ($h^*\leq 1$). As the transformation reaches the final stage, it becomes more difficult to satisfy the assumptions of JMAK theory including the uniform distribution of nuclei and random impingement, owing to the fact that the majority of the available untransformed space is fragmented to the small pieces, scattered over the entire system. Under these circumstances, the probability of having new nuclei in the system is quite rare. It has been reported analytically and

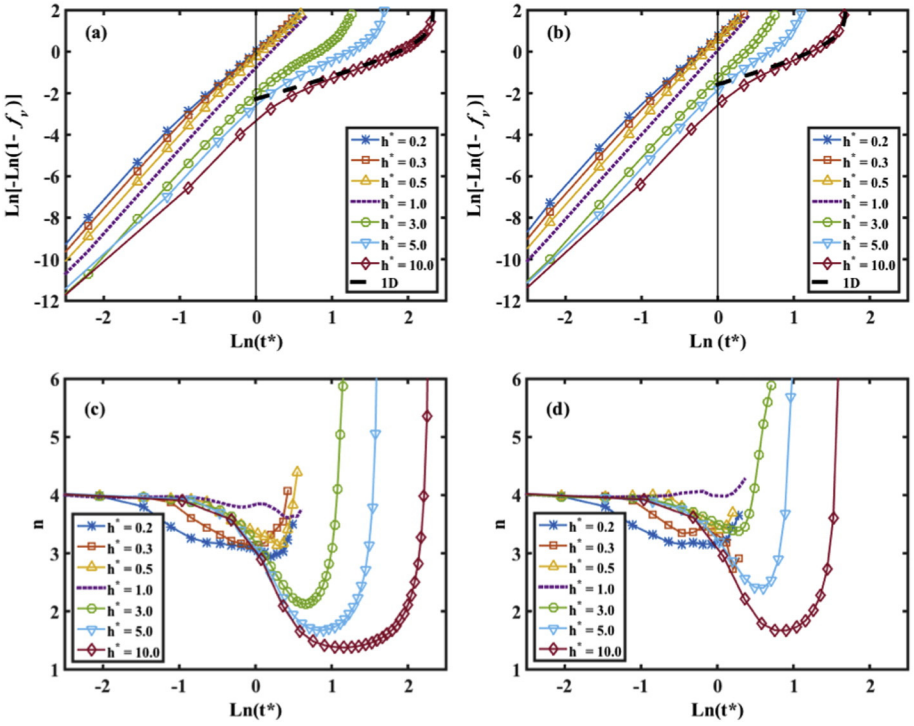

Fig. 8. Evolution of the Avrami exponent as a function of h^* for the surface nucleation case. Average values over 40 runs with different random initial configurations are displayed. (a) Avrami plot (1-surface case). (b) Avrami plot (2-surface case). Dashed line represents solution for a 1D planar front at $h^*=10$. Fine solid line at $\ln[t^*]=0$, highlights different y-intercept as an indication of different rate constant. (c) Avrami exponent vs. natural log of time (1-surface case). (d) Avrami exponent vs. natural log of time (2-surface case).

experimentally that this situation leads to a deviation from the ideal JMAK behavior as well [13,14,24,27,35]. This phenomenon is also consistent with the nucleation rate becoming discrete in finite systems unlike an infinite system, which the nucleation rate remains continuous [39]. Hence, as the system size becomes larger, the probability of continuous nucleation toward the end of transformation increases and the Avrami exponent goes to a constant value, as being predicted in Očenášek et al.'s analytical model [17]. Fig. 9 shows the effect of system size on the evolution of local Avrami exponent over the time for the extreme case of $h^*=0.2$. Evidently increasing the system size results in a volume fraction evolution that yields a lower Avrami exponent in the final stages of the transformation. However, the simulation doesn't show any significant changes in the total transformation time ($\approx$99% completion of transformation) or structural property (average grain size and the grain size distribution) for different system size.

The non-linear Avrami plot is more evident in results of the heterogeneous nucleation from the surfaces (Section 4.2). The results for $h^*\leq 1$ demonstrate fairly similar behavior to homogeneous case and can be explained by the same logic as before. But more interestingly the effect of film thickness on non-linearity of the Avrami regime is more pronounced for $h^*>1$ (see Figs. 7 & 8). As mentioned earlier for thicker films, transformation occurs via 3D growth at primary stage and after passing multiple intermediate stages, continues through 1D growth. This transition in growth dimensionality causes non-constant Avrami exponent. Increasing the film thickness leads to more available space for intermediate stages, which introduces more curvature to the Avrami plot.

Another parameter involved in JMAK equation is the rate constant, which is frequently overlooked in the analysis of the growth dimensionality. In Figs. 3(b) and 8(a, b) it is clearly illustrated that film thickness has direct effect on rate constant as each line crosses the y-axis at $\ln[t^*]=0$ with a different value, despite the fact that all simulations are performed with the same initial conditions ($\dot{N}_V{}^*$ and v^*) and by the JMAK analysis, are supposed to show identical rate constants as shown in Fig. 1(b). In the derivation of the JMAK equation, the rate constant accounts for the evolution of the extended volume (ignoring the impingement), which makes it as significant as Avrami exponent in study of transformation dimensionality. Furthermore, since the rate constant is also used to determine the activation energy of the transformation, care must be taken to incorporate this size effect in calculation [35,40]. It can be difficult to determine $\ln[t^*]=0$ experimentally, so as discussed in Section 4.1, we can use the measured average grain size and film thickness to determine characteristic length of the system. Then use that as a criterion to determine the dominant growth dimensionality based on film thickness in thin film phase transformations under a constant nucleation rate.

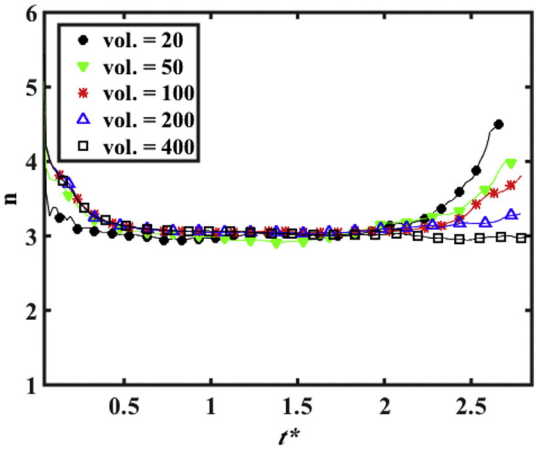

Fig. 9. Evolution of Avrami exponent over time for bulk nucleation case ($h^*=0.2$). Depiction of an evident departure from the exponent of 3 at final stage that is expected in infinite films. Average values over 40 runs with different random initial configurations are displayed.

6. Conclusions

The level-set method has been employed to simulate an isothermal phase transformation in thin films under constant nucleation rate and isotropic growth. Results produced by this simulation method are then used to investigate the effect of a finite size domain and heterogeneous nucleation on the kinetic behavior of the transformation using the framework of the classic JMAK theory. Kinetic parameters including the nucleation rate and interface velocity encompassed in characteristic length and time scales of the system are used to conduct a systematic study of phase transformation kinetics in bulk and surface nucleation cases. It is confirmed that both finite size domain and heterogeneous nucleation on the surface result in a reduced Avrami exponent. During homogenous nucleation, only at sufficiently small film thicknesses ($h^*\leq 1$) a non-linear regime in Avrami plot is observable. However, the effect of heterogeneous nucleation on the non-linearity of the Avrami plot is more pronounced for thicker films ($h^*>1$). It is shown that the Avrami exponent can acquire different values over the course of the transformation in thin films. The single value of the Avrami exponent does not, therefore, always represent the dimensionality of the new phase growth. The rate constant also varies strongly with film thickness and nucleation heterogeneity. Thus, unless these variations of the rate constant are considered, the temperature dependence of this parameter will not yield the correct activation energy for the transformation. The grain size distribution at the end of the transformation are obtained for various film thicknesses and is used to show the dependence of the average grain size on the film thickness. The connection between these two parameters is then used to determine the characteristic length of the system that can be used as a parameter for further analysis. Tracking the change in the rate constant and the grain size distribution lead to a new criterion for determining the dominant growth dimensionality in thin film phase transformations, rather than the classical non-constant Avrami exponent. This criterion identifies the growth dimensionality for a film thickness less than characteristic length ($h^*<1$) as 2D dominant and for thickness greater than characteristic length ($h^*>1$) as 3D dominant. However, the growth is never exactly 2D or 3D except for extremely thin 2D systems or nearly 3D volumes.

Acknowledgment

The support of the NSF-MRSEC at Northwestern, DMR-1121262, is gratefully appreciated.

References

[1] D.Z. Hu, X.M. Lu, J.S. Zhu, F. Yan, Study on the crystallization by an electrical resistance measurement in Ge2Sb2Te5 and N-doped Ge2Sb2Te5 films, J. Appl. Phys. 102 (2007) 113507, http://dx.doi.org/10.1063/1.2818104.
[2] G. Gurato, D. Gaidano, R. Zannetti, Influence of nucleating agents on the crystallization of 6-polyamide, Makromol. Chem. 179 (1978) 231–245, http://dx.doi.org/10.1002/macp.1978.021790123.
[3] G. Ghosh, M. Chandrasekaran, L. Delaey, Isothermal crystallization kinetics of Ni24Zr76 and Ni24(Zr-X)76 amorphous alloys, Acta Metall. Mater. 39 (1991) 925–936, http://dx.doi.org/10.1016/0956-7151(91)90292-9.
[4] J.C. Holzer, K.F. Kelton, Kinetics of the amorphous to icosahedral phase transformation in Al-Cu-V alloys, Acta Metall. Mater. 39 (1991) 1833–1843, http://dx.doi.org/10.1016/0956-7151(91)90152-Q.
[5] M. Wang, H. Lei, Y. Seki, S. Seki, Y. Sawada, Y. Hoshi, et al., Thermal crystallization kinetic and electrical properties of partly crystallized amorphous indium oxide thin films sputtering deposited in the presence or the absence of water vapor, J. Therm. Anal. Calorim. 111 (2013) 1457–1461, http://dx.doi.org/10.1007/s10973-012-2526-9.
[6] M. Avrami, Granulation, phase change, and microstructure kinetics of phase change. III, J. Chem. Phys. 9 (1941) 177–184, http://dx.doi.org/10.1063/1.1750872.
[7] M. Avrami, Kinetics of phase change. II transformation-time relations for random distribution of nuclei, J. Chem. Phys. 8 (1940) 212–224, http://dx.doi.org/10.1063/1.1750631.

[8] M. Avrami, Kinetics of phase change. I. General theory, J. Chem. Phys. 7 (1939) 1103–1112, http://dx.doi.org/10.1063/1.1750380.
[9] A.N. Kolmogorov, On the statistical theory of the crystallization of metals, Bull. Acad. Sci. USSR, Math. Ser. 1 (1937) 355–359.
[10] W.A. Johnson, R.F. Mehl, Reaction kinetics in processes of nucleation and growth, Trans. AIME 135 (1939) 396–415.
[11] A.K. Jena, M.C. Chaturvedi, Phase Transformation in Materials, Prentice Hall, 1992.
[12] M. Weinberg, R. Kapral, Phase transformation kinetics in finite inhomogeneously nucleated systems, J. Chem. Phys. 91 (1989) 7146–7152, http://dx.doi.org/10.1063/1.457330.
[13] L.E. Levine, K.L. Narayan, K.F. Kelton, Finite size corrections for the Johnson–Mehl–Avrami–Kolmogorov equation, J. Mater. Res. 12 (1997) 124–132, http://dx.doi.org/10.1557/JMR.1997.0020.
[14] M.T. Todinov, On some limitations of the Johnson–Mehl–Avrami–Kolmogorov equation, Acta Mater. 48 (2000) 4217–4224, http://dx.doi.org/10.1016/S1359-6454(00)00280-9.
[15] V.I. Trofimov, I.V. Trofimov, J.-I. Kim, Finite size effects in phase transformation kinetics in thin films and surface layers, Nuclear Instruments and Methods in Physics Research Section B: Beam Interactions with Materials and Atoms. 216 (2004) 334–339, http://dx.doi.org/10.1016/j.nimb.2003.11.057.
[16] Alekseechkin, On the kinetics of phase transformation of small particles in Kolmogorov's model, Condensed Matter Physics 11 (2008) 597, http://dx.doi.org/10.5488/CMP.11.4.597.
[17] J. Očenášek, P. Novák, S. Agbo, Finite-thickness effect on crystallization kinetics in thin films and its adaptation in the Johnson–Mehl–Avrami–Kolmogorov model, J. Appl. Phys. 115 (2014) 043505, http://dx.doi.org/10.1063/1.4862858.
[18] J.M. Schultz, Effect of specimen thickness on crystallization rate, Macromolecules 29 (1996) 3022–3024.
[19] N. Billon, J.M. Escleine, J.M. Haudin, Isothermal crystallization kinetics in a limited volume. A geometrical approach based on Evans' theory, Colloid Polym. Sci. 267 (1989) 668–680, http://dx.doi.org/10.1007/BF01524369.
[20] J.M. Escleine, B. Monasse, E. Wey, J.M. Haudin, Influence of specimen thickness on isothermal crystallization kinetics. A theoretical analysis, Colloid Polym. Sci. 262 (1984) 366–373, http://dx.doi.org/10.1007/BF01410254.
[21] J.M. Rickman, W.S. Tong, K. Barmak, Impact of heterogeneous boundary nucleation on transformation kinetics and microstructure, Acta Mater. 45 (1997) 1153–1166, http://dx.doi.org/10.1016/S1359-6454(96)00245-5.
[22] S.-B. Lee, J.M. Rickman, K. Barmak, Phase transformation kinetics and self-patterning in misfitting thin films, Acta Mater. 51 (2003) 6415–6427, http://dx.doi.org/10.1016/j.actamat.2003.08.021.
[23] K. Sekimoto, Evolution of the domain structure during the nucleation-and-growth process with non-conserved order parameter, Physica A: Statistical Mechanics and Its Applications. 135 (1986) 328–346, http://dx.doi.org/10.1016/0378-4371(86)90146-9.
[24] E.L. Pang, N.Q. Vo, T. Philippe, P.W. Voorhees, Modeling interface-controlled phase transformation kinetics in thin films, J. Appl. Phys. 117 (2015) 175304, http://dx.doi.org/10.1063/1.4919725.
[25] M.C. Weinberg, Surface nucleated transformation kinetics in 2- and 3-dimensional finite systems, J. Non-Cryst. Solids 134 (1991) 116–122, http://dx.doi.org/10.1016/0022-3093(91)90018-2.
[26] M.C. Weinberg, Non-isothermal surface nucleated transformation kinetics, J. Non-Cryst. Solids 151 (1992) 81–87, http://dx.doi.org/10.1016/0022-3093(92)90012-9.
[27] N.X. Sun, X.D. Liu, K. Lu, An explanation to the anomalous avrami exponent, Scr. Mater. 34 (1996) 1201–1207, http://dx.doi.org/10.1016/1359-6462(95)00657-5.
[28] For surface nucleation cases, $\lambda = (\dot{N}_A/v)^{-1/3}$ where, $\dot{N}_A$ is a nucleation rate per area per time.
[29] S. Osher, R. Fedkiw, Level Set Methods and Dynamic Implicit Surfaces, Springer New York, New York, NY, 2003 (http://link.springer.com/10.1007/b98879 accessed April 15, 2015).
[30] J.A. Sethian, Level Set Methods and Fast Marching Methods: Evolving Interfaces in Computational Geometry, Fluid Mechanics, Computer Vision, and Materials Science, Cambridge University Press, 1999.
[31] J.E. Taylor, J.W. Cahn, C.A. Handwerker, Overview No. 98 I—geometric models of crystal growth, Acta Metall. Mater. 40 (1992) 1443–1474, http://dx.doi.org/10.1016/0956-7151(92)90090-2.
[32] G. Russo, P. Smereka, A level-set method for the evolution of faceted crystals, SIAM J. Sci. Comput. 21 (2000) 2073–2095, http://dx.doi.org/10.1137/S1064827599351921.
[33] P. Smereka, X. Li, G. Russo, D.J. Srolovitz, Simulation of faceted film growth in three dimensions: microstructure, morphology and texture, Acta Mater. 53 (2005) 1191–1204, http://dx.doi.org/10.1016/j.actamat.2004.11.013.
[34] Z.J. Liu, J. Ouyang, W. Zhou, X.D. Wang, Numerical simulation of the polymer crystallization during cooling stage by using level set method, Comput. Mater. Sci. 97 (2015) 245–253, http://dx.doi.org/10.1016/j.commatsci.2014.10.038.
[35] A. Calka, A.P. Radlinski, The local value of the Avrami exponent: a new approach to devitrification of glassy metallic ribbons, Mater. Sci. Eng. 97 (1988) 241–246, http://dx.doi.org/10.1016/0025-5416(88)90050-X.
[36] D.J. Rowenhorst, A.C. Lewis, G. Spanos, Three-dimensional analysis of grain topology and interface curvature in a β-titanium alloy, Acta Mater. 58 (2010) 5511–5519, http://dx.doi.org/10.1016/j.actamat.2010.06.030.
[37] P. Revesz, The Laws of Large Numbers, Probability and Mathematical Statistics, Academic Press, New York and London, 1968.
[38] D.W. Scott, On optimal and data-based histograms, Biometrika 66 (1979) 605–610, http://dx.doi.org/10.2307/2335182.
[39] A.V. Teran, A. Bill, R.B. Bergmann, Time-evolution of grain size distributions in random nucleation and growth crystallization processes, Phys. Rev. B 81 (2010) 075319, http://dx.doi.org/10.1103/PhysRevB.81.075319.
[40] X. Wang, M. Rein, J.J. Vlassak, Crystallization kinetics of amorphous equiatomic NiTi thin films: effect of film thickness, J. Appl. Phys. 103 (2008) 023501, http://dx.doi.org/10.1063/1.2829811.